

Shape and orientation effects on the ballistic phonon thermal properties of ultra-scaled Si nanowires

Abhijeet Paul,^{1, a)} Mathieu Luisier,¹ and Gerhard Klimeck¹

School of Electrical and Computer Engineering, Network for Computational Nanotechnology, Purdue University, West Lafayette, Indiana, USA, 47907.

(Dated: 1 March 2022)

The effect of geometrical confinement, atomic position and orientation of Silicon nanowires (SiNWs) on their thermal properties are investigated using the phonon dispersion obtained using a Modified Valence Force Field (MVFF) model. The specific heat (C_v) and the ballistic thermal conductance (κ_l^{bal}) shows anisotropic variation with changing cross-section shape and size of the SiNWs. The C_v increases with decreasing cross-section size for all the wires. The triangular wires show the largest C_v due to their highest surface-to-volume ratio. The square wires with [110] orientation show the maximum κ_l^{bal} since they have the highest number of conducting phonon modes. At the nano-scale a universal scaling law for both C_v and κ_l^{bal} are obtained with respect to the number of atoms in the unit cell. This scaling is independent of the shape, size and orientation of the SiNWs revealing a direct correlation of the lattice thermal properties to the atomistic properties of the nanowires. Thus, engineering the SiNW cross-section shape, size and orientation open up new ways of tuning the thermal properties at the nanometer regime.

^{a)}Electronic mail: abhijeet.rama@gmail.com

I. INTRODUCTION

The increasing variety of application of Silicon nanowires (SiNWs) ranging from MOSFETs¹ to rechargeable batteries², thermoelectric (TE) devices³, bio-sensors⁴, solar cells⁵, etc., requires a good understanding of the lattice thermal properties. Thermal requirements can be very contrasting depending on the type of applications, for eg. MOSFETs will require heat dissipation for better performance whereas thermoelectric devices require low thermal conductivity to maintain a good temperature gradient for higher TE efficiency⁶.

Improvement in the process technologies have led to the fabrication of SiNWs with different shapes, sizes and channel orientations^{3,7-9}. SiNWs with channel orientations along [100], [110] and [111] are the most commonly manufactured ones. At the nanometer scale, strong geometrical confinement, atomic positions and increased surface-to-volume ratio (SVR) play significant roles in determining the thermal properties of the SiNWs^{6,10,11}.

Thermal transport measurements using techniques like the 3ω method¹² and thermo-reflectance¹³ have led to a good understanding of the heat flow in large nanowires (diameter $> 30\text{nm}$). However, the physics of heat flow in ultra-scaled SiNWs is still not well understood⁶. The phonon spectra of SiNWs can provide a theoretical estimate of heat transport through ultra-scaled structured since phonons (lattice vibrations) are responsible for carrying most of the heat in semiconductors^{6,10,11,14}.

In this paper we theoretically explore the effect of (i) cross-section geometry, (ii) cross-section size, and (iii) wire orientation of ultra-scaled SiNWs on the thermal properties such as the ballistic thermal conductance (κ_l^{bal}) and the specific heat (C_v). Furthermore, analytical expressions for the variation of these physical quantities with size for each cross-section shape and orientation are provided to allow for a compact modeling representation of thermal properties to be used in simulators like Thermal-Spice¹⁵ and Thermoelectric module simulator¹⁶.

The thermal properties of SiNWs differ considerably from bulk Si^{6,8}. The transition from the particle to wave nature of heat transport with structural miniaturization calls for improved heat transport models. The traditional continuum models for thermal conductivity by Callaway¹⁷ and Holland¹⁸ are based on the Debye limit for phonons, sound velocity and many other parameters, which render these models quite cumbersome at the nanoscale, as discussed by Mingo et al¹⁰. The dependence of continuum models on a large set of fit-

ting parameters make them unsuitable for predicting the lattice thermal properties with dimensional scaling. This limitation can be overcome by atomistic models which automatically take into account the effects of structural miniaturization like geometrical confinement, orientation effects, cross-sectional shape and surface-to-volume ratio effects^{10,11}.

Theoretical estimates of the thermal conductivity and the specific heat using phonon spectra have been addressed in the literature in the past. Calculations of thermal conductivity using the full phonon spectra of large to medium sized SiNWs along certain specific orientations have been performed^{10,19}. The influence of surface roughness on nanowires has been studied in Refs.²⁰⁻²². A study of specific heat in [111] SiNWs is reported in Ref.²³. Mingo et. al theoretically bench-marked the thermal conductivity of large SiNWs (diameter $\geq 34\text{nm}$)¹⁰ and also studied the effect of amorphous coating on the thermal conductivity of SiNWs¹¹. A complete study of orientation effects on the thermal conductivity of SiNW has been provided in Ref.⁶. The thermal conductivity of Si nano-clusters^{24,25} and hollow Si nanowires^{14,26} has also been studied.

In this work we utilize a semi-empirical phonon model to perform thermal calculations. The phonon dispersion is obtained using a Modified Valence Force Field (MVFF) model^{27,28}. The continuum models^{17,18} though computationally simpler and faster, lack the proper physics to extend them to nanostructures due to the use of open fitting parameters²⁹. The first principles based models^{30,31} are limited to extremely small structures ($W < 2\text{nm}$) with few thousand atoms, and are computationally very expensive. The choice of the MVFF model is guided by the following factors, (i) an adequate amount of physics to understand the thermal properties, and (ii) a lower computational cost thus, allowing the model to handle up to few million atoms for phonon calculations in realistic structures³². At the same time the MVFF model also explains the experimental phonon and elastic properties in zinc-blende materials very well^{27,33,34}.

The emphasis of this work is to purely understand the atomistic effects on the thermal properties of ultra-scaled SiNWs such as the effect of the surfaces and atomic coordination number. This understanding is further translated into analytical equations allowing easy usage for other thermal modeling like thermo-electric circuit simulations which require C_v and κ_l as input¹⁶. Scattering effects are dominating at the nanometer scale in determining the lattice thermal conductivity. However, scattering effects have been neglected in the present study in order to understand the geometric and atomistic effects which will be

otherwise convoluted by scattering. Also the ballistic phonon transport can be supported in SiNWs with width smaller than 20nm as pointed in Ref.³⁵. The scattering effects could be studied as a future work.

The paper is organized as follows. Section II provides a brief description of the MVFF model for the calculation of phonons in SiNWs, the calculation of thermal properties (Sec. II B) and details of the SiNWs used for the study (Sec. II C). The effect of cross-section shape, size and wire orientation on the specific heat and thermal conductance are discussed in Sec. III A and Sec. III B, respectively. This is followed by a discussion on the atomistic effects on the thermal properties in Sec. III C. Conclusions are summarized in Sec. IV.

II. THEORY AND APPROACH

A. MVFF Phonon model

In the MVFF model, the phonon frequencies are calculated from the forces acting on atoms produced by finite displacements of the atoms from their equilibrium positions in a crystal³⁰. First the total potential energy of the solid (U) is estimated from the restoring force(F). In the MVFF model, U is approximated as²⁸,

$$U \approx \frac{1}{2} \sum_{i \in N_A} \left[\sum_{j \in nn(i)} U_{bs}^{ij} + \sum_{\substack{j \neq k \\ j, k \in nn(i)}} (U_{bb}^{jik} + U_{bs-bs}^{jik} + U_{bs-bb}^{jik}) + \sum_{\substack{j \neq k \neq l \\ j, k, l \in COP_i}} U_{bb-bb}^{jkl} \right], \quad (1)$$

where N_A , $nn(i)$, and COP_i represent the total number of atoms in one unit cell, number of nearest neighbors for atom ‘i’, and the coplanar atom groups for atom ‘i’, respectively. The first two terms U_{bs}^{ij} and U_{bb}^{jik} represent the elastic energy obtained from bond stretching and bending between atoms connected to each other³⁶. The terms U_{bs-bs}^{jik} , U_{bs-bb}^{jik} , and U_{bb-bb}^{jkl} represent the cross bond stretching²⁷, the cross bond bending-stretching³³, and the coplanar bond bending²⁷ interactions, respectively. The detailed procedure for obtaining the phonon spectra in bulk Si and NWs are outlined in Ref.^{28,37}.

B. Lattice thermal properties

The complete phonon dispersion provides information about the thermal properties of nanostructures^{6,10,11}. The constant volume temperature (T) dependent specific heat ($C_v(T)$) can be evaluated using the following relation³⁸,

$$C_v(T) = \left(\frac{k_B}{m_{uc}}\right) \cdot \sum_{n,q} \left[\frac{\left(\frac{\hbar\omega_{n,q}}{k_B T}\right) \cdot \exp\left(\frac{-\hbar\omega_{n,q}}{k_B T}\right)}{\left[1 - \exp\left(\frac{-\hbar\omega_{n,q}}{k_B T}\right)\right]^2} \right] [J/kgK], \quad (2)$$

where k_B , \hbar and m_{uc} are the Boltzmann's constant, reduced Planck's constant, and the mass of the SiNW unit cell in kg, respectively. The quantity $\omega_{n,q}$ is the phonon frequency associated with the branch 'n' and crystal momentum vector 'q'.

For a semiconductor slab/wire with a small temperature difference ΔT between its two extremities, the thermal conductance (κ_l^{bal}) is obtained using Landauer's method³⁹ as^{6,10,11},

$$\kappa_l^{bal}(T) = \hbar \int_0^{\omega_{max}} T(\omega) \cdot M(\omega) \cdot \omega \cdot \frac{\partial}{\partial T} \left[\left(\exp\left(\frac{\hbar\omega}{k_B T}\right) - 1 \right)^{-1} \right] \cdot d\omega [W/K], \quad (3)$$

The term $M(\omega)$ is the number of phonon modes at frequency ω and $T(\omega)$ is the transmission for each mode. For ballistic conductance each mode transmits with a probability of 1 while for coherent scattering dominated conductance the transmission value is less than 1.

C. Si Nanowire details

In this study, four types of cross-section shapes for [100] SiNWs have been considered namely, (a) circular, (b) hexagonal, (c) square and (d) triangular (Fig. 1). Square SiNWs with [110] and [111] channel orientations have been studied too (Fig. 2). The feature size is determined by the width parameter W. The value of W is varied from 2 to 6 nm. The confinement direction of the SiNWs are along Y and Z. The heat transport direction is along X. The surface atoms are allowed to vibrate freely without any passivating species. These wires are assumed to have a tetrahedral geometry. It has been shown that wires with

diameter below 2nm tend to lose the tetrahedral structure^{40,41} due to surface pressure and internal strain.

III. RESULTS AND DISCUSSION

In this section the results on the effect of cross-section shape, size and orientation on the thermal properties of SiNWs are presented and discussed. All the thermal quantities are calculated at 300K. However, the analysis holds for any temperature (T) where the anharmonic phonon effects are small. For $T < T_{Debye}$ the anharmonic interactions are quite small¹⁴. For bulk Si, $T_{Debye} \sim 725\text{K}$ ⁴² and it further increases for SiNWs⁴⁰.

A. Specific heat in SiNWs

Influence of the shape and size on C_v : The C_v of SiNWs increases with decreasing cross-section size in all the wire shapes (Fig. 3a). The size dependence of C_v can be approximated by the following relation²³,

$$C_v(W) = C_v^{bulk} + \frac{A}{W}, \quad (4)$$

where, A is a fitting parameter extracted from the linear fit of the numerical simulations. Table I shows the value of C_v^{bulk} and A for each geometry. As $W \rightarrow \infty$ (increasing cross-section size), the C_v of all the SiNWs converges to a fixed value of ~ 681 J/kg.K which is reasonably close to the experimental C_v value for bulk Si (~ 682 J/Kg.K as provided in Refs.^{23,43}). The triangular wires show the maximum C_v for all the W value, whereas the other shapes show similar C_v values at any given cross-section size (Fig. 3a).

The plot of $\Delta C_v (=C_v^{wire} - C_v^{bulk})$ vs. SVR (SVR = Total surface Atoms/Total atoms in unit cell) shows a linear behavior (Fig. 3b), which can be represented as,

$$C_v^{wire} \approx m_c \times \text{SVR} + C_v^{bulk}, \quad (5)$$

where m_c describes the additional contribution to the C_v of the SiNWs with increasing surface-to-volume ratio. The value of m_c is positive for all the wire shapes (Fig. 3b) which corroborates the fact that specific heat increases with increasing surface area²³. Different

coordination number of surface atoms for the various cross-section shapes result in different m_c values which depict the atomistic effect on the C_v value in ultra-scaled SiNWs.

The C_v increase with decreasing W can be attributed to two phenomena, (i) phonon confinement due to small cross-section size and (ii) an increased surface-to-volume ratio (SVR) in smaller wires^{23,37}. With increasing geometrical confinement (smaller cross-section size) the phonon bands are more separated in energy³⁷ which makes only the few lower energy bands active at a given temperature (see Eq. 2). Thus, more energy is needed to raise the temperature of the smaller wires.

The shape dependence of the C_v can be understood from Eq. 5. The variation of (i) SVR, and (ii) m_c with W for different shapes decide the eventual C_v order. Figure 4(a) shows that triangular wires have the maximum SVR while the other shapes have similar SVR at a fixed W . The increasing SVR results in a higher phonon density of states (DOS) associated with the wire surface, which further enhances the specific heat with decreasing wire cross-section²³. The square wires provide the largest surface contribution to C_v as depicted by the variation in m_c ($\Delta C_v/\text{SVR}$) (Fig. 4b). An optimal value of SVR and m_c in SiNWs will maximize the C_v . The $\text{SVR} \times m_c$ value has the following order, triangle (~ 36) > hexagonal (~ 29) > square (~ 27) > circular (~ 26). Thus, triangular wires depict the highest C_v due to the highest SVR. However, the trends for SVR ($\text{SVR}_{sq} < \text{SVR}_{hex} < \text{SVR}_{ci}$) and m_c ($m_c^{sq} > m_c^{hex} > m_c^{ci}$) are opposite for the other shapes, hence resulting in almost similar C_v values. The C_v values have the following shape order in [100] SiNWs: *triangular* > *hexagonal* \approx *square* \approx *circular*.

Influence of orientation on C_v : The specific heat is also a function of the SiNW orientation (Fig. 5a). The C_v varies inversely with W , similar to the trend extracted from different shapes (Eq. 4). The width parameters (Eq. 4) for the variation of C_v with orientation are provided in Table II. The ΔC_v value again shows a linear variation with SVR for different wire orientations (Fig. 5b). The C_v has the following trend with orientation for different cross-section sizes, $C_v^{100} > C_v^{110} > C_v^{111}$. This trend can be explained again by looking at the impact of (i) SVR and (ii) m_c (Eq. 5) on the overall C_v value. The SVR shows the following order with W , $\text{SVR}^{111} > \text{SVR}^{110} > \text{SVR}^{100}$ (inc. of $\sim 1.2\times$ from [100] to [111]) as illustrated in Fig. 6a. However, m_c shows the following order with W , $m_c^{100} > m_c^{110} > m_c^{111}$ (dec. of $\sim 1.7\times$ from [100] to [111]) (Fig. 6b). *The larger surface to volume ratio plays the main role in deciding the C_v trend for SiNWs with different orientations.*

B. Ballistic thermal conductance of SiNWs

The thermal conductance indicates how a structure can carry heat. For high thermoelectric efficiency (ZT) a small thermal conductance is needed^{10,11,44} whereas for CMOS transistors a high κ_l is preferred to evacuate the heat. The cross-section shape, size and wire orientation of SiNWs can be used to tune their the thermal conductance.

Influence of the shape and size on κ_l^{bal} : The ballistic thermal conductance (κ_l^{bal}) for 4 different shapes (Fig. 1) of [100] SiNWs are calculated as shown in Fig. 7a. The κ_l^{bal} can be fitted according to the following size (W) relation,

$$\kappa_l^{bal}(W) = \kappa_0 \left(\frac{W}{a_0} \right)^d, \quad (6)$$

where a_0 is the silicon lattice constant (0.5431 nm), d is a power exponent, and κ_0 is a constant of proportionality. The values of 'd' and κ_0 for different wires shapes are provided in Table III. The value of d varies between 1.92 and 2.011 which implies that κ_l^{bal} has a similar size dependence for all the wire shapes. However, the pre-factor value (κ_0) reflects the shape dependence. This pre-factor has the same ordering as the thermal conductance ordering (Fig. 7a and Table III).

The ballistic thermal conductance exhibits a linear behavior with the number of atoms per unit cell (NA) as depicted in Fig. 7b. This linear relation can be approximated by the following equation,

$$\kappa_l^{bal} \approx m_k \times NA + \kappa_l^{bal}(0), \quad (7)$$

where the slope m_k represents the average contribution from each atom in the unit cell to κ_l^{bal} and $\kappa_l^{bal}(0)$ is the thermal conductance at NA = 0. The value of $\kappa_l^{bal}(0)$ is zero within numerical error ($\kappa_l^{bal}(0) \approx 1e-7$) which is expected for NA = 0. The value of m_k takes into account the surface, shape and atomic effects since the calculation procedure involves the complete phonon dispersion. This relation shows a direct correlation of the atomistic effects to the ballistic thermal conductance.

The size dependence can be explained by the fact that the larger wires have (i) more phonon sub-bands resulting in higher number of modes ($M(\omega)$ in Eq. 3) and (ii) a higher acoustic sound velocity which is responsible for a larger heat conduction in these SiNWs³⁷.

The shape dependence can be explained as an interplay of two effects, (i) the total number of atoms (NA) present in the unit cell of SiNWs, and (ii) the average contribution of every

atom towards κ_l^{bal} . For a fixed cross-section size W , the NA ordering is $NA_{sq} > NA_{ci} > NA_{hex} > NA_{Teri}$ (Fig. 8a). The total number of phonon branches are $3 \times NA$, due to the three degrees of freedom associated with each atom²⁸. The number of phonon modes ($M(\omega)$) is directly proportional to the phonon energy sub-bands. The contribution per atom to the thermal conductance (m_k) stays almost constant with the wire cross-section size for a given shape (Fig. 8b). *Since, the values of m_k are quite similar for all the cross-section shapes, the ordering of NA with shape governs the dependence of κ_l^{bal} on the cross-section shape.*

Influence of wire orientation on κ_l^{bal} : The thermal conductance is anisotropic in SiNWs with the following order, $\kappa_l^{110} > \kappa_l^{100} > \kappa_l^{111}$ (Fig. 9a). This result is similar to the one reported in Ref.⁶. The κ_l value exhibits a linear variation with NA for all the wire orientations (Fig. 9b). The width parameters for the thermal conductance (Eq. 6) for different wire orientations are provided in Table IV. The order of the ballistic thermal conductance with W for different orientations can be understood by the product of $NA \times m_k$ (P_{nm}). The NA has the following variation, $NA^{111} > NA^{110} > NA^{100}$ (Fig. 10a), whereas m_k depicts the following order $m_k^{100} > m_k^{110} > m_k^{111}$ (Fig.10b). These two orders are opposite to each other. However, the product shows the following order, $P_{nm}^{110} > P_{nm}^{100} > P_{nm}^{111}$. Thus, [110] wires give the highest κ_l due to the optimal value of NA and m_k .

An important point to note is that κ_l^{bal} is expected to decrease further in smaller wires due to phonon scattering by other phonons, interfaces and boundaries^{10,11} which are neglected in this present study. The main idea here is to understand the geometrical effects on the phonon dispersion and the lattice thermal properties of these small nanowires which is attributed to (i) the modification of the phonon dispersion, and (ii) phonon confinement effects in the coherent phonon transport regime.

C. Discussion

In this work, all the thermal properties are shown to scale with W . Also NA depends on W as follows,

$$NA \propto W^\gamma, \quad (8)$$

where $\gamma > 0$. So using Eq. (8), (4) and (6) can be recasted in terms of NA as,

$$\Delta C_v(NA) = C_0 \cdot (NA)^{\frac{-1}{\gamma}} \quad (9)$$

$$= C_0 \cdot (NA)^{-\eta}$$

$$\kappa_l^{bal}(NA) = K_0 \cdot (NA)^{\frac{d}{\gamma}} \quad (10)$$

$$= K_0 \cdot (NA)^\rho,$$

where, C_0 and K_0 are the pre-factors. Thus, a universal power law can be derived for the thermal properties depending on the number of atoms per unit cell (NA) which represents the atomistic effect on the thermal quantities. In these SiNWs, $1.98 \leq \gamma \leq 2.1$ which provides the limits for ρ and η ,

$$\rho \in [0.93, 1.03] \quad (11)$$

$$\eta \in [0.48, 0.50] \quad (12)$$

The variation in the thermal conductance with NA is illustrated on a log-log scale in Fig. 11a. All the SiNWs depict almost the same power law with an average exponent value of ~ 0.97 , which is in the limit derived in Eq. 11. Similarly the variation in C_v with NA is plotted on a log-log scale in Fig. 11b. All the SiNWs used in this study show the same power law (Eq. 9) with an average exponent of -0.51, which is in the limit derived in Eq. 12. Thus, the thermal quantities show a universal power law behavior with the number of atoms in the unit cell (NA) irrespective of the details of the unit cell. The details of shape and orientation are embedded in the pre-factors C_0 and K_0 (Eq. 9 and 10).

The relationship of C_v and κ_l to the shape, size and orientation of SiNWs have been provided explicitly in Eqs. (4), (5), (6), and (7). These closed form analytical expressions are very handy for the compact modeling of the thermal and thermoelectric properties of SiNWs^{15,16}. Since these expression are derived from physics-based model, they capture the important geometrical and atomistic effects, thus enabling fast modeling of realistic systems.

IV. CONCLUSIONS

We have shown the application of the MVFF model for the calculation of the thermal properties of SiNWs. It has been shown that at the nanometer scale these thermal prop-

erties are quite sensitive to the wire cross-section size, shape, and orientation. Analytical expressions for the size dependence of the thermal properties of SiNWs of different cross-section shape and channel orientation have been provided. They can be used as component for the compact modeling of the thermal properties of ultra-scaled SiNWs. It has been demonstrated that all the SiNWs follow a universal power law for the specific heat and the thermal conductance which reveals the impact of the atomistic details on these properties. The triangular SiNWs show a high C_v and low κ_l , thus making them good candidates for thermoelectric devices. The [110] oriented square Si nanowires are better in terms of heat dissipation due to their high thermal conductance and are therefore good candidates for transistors from a heat management point of view.

ACKNOWLEDGMENTS

The authors acknowledge financial support from MSD Focus Center, under the Focus Center Research Program (FCRP), a Semiconductor Research Corporation (SRC) entity, Nanoelectronics Research Initiative (NRI) through the Midwest Institute for Nanoelectronics Discovery (MIND), NSF (Grant No. OCI-0749140) and Purdue University. Computational support from nanoHUB.org, an NCN operated and NSF (Grant No. EEC-0228390) funded project is also gratefully acknowledged.

REFERENCES

- ¹N. Singh, A. Agarwal, L. K. Bera, T. Y. Liow, R. Yang, S. C. Rustagi, C. H. Tung, R. Kumar, G. Q. Lo, N. Balasubramanian, and D. L. Kwong, *IEEE Electron Dev. Lett.* **27**, 383 (2006).
- ²C. K. Chan, H. Peng, G. Liu, K. McIlwrath, X. F. Zhang, R. A. Huggins, and Y. Cui, *Nature Nanotechnology* **3**, 31 (2007).
- ³A. I. Hochbaum, R. Chen, R. D. Delgado, W. Liang, E. C. Garnett, M. Najarian, A. Majumdar, and P. Yang, *Nature* **451**, 163 (2008).
- ⁴X. P. A. Gao, G. Zheng, and C. M. Lieber, *Nano Letters* **10**, 547 (2010).
- ⁵E. Garnett and P. Yang, *Nano Letters* **10**, 1082 (2010).
- ⁶T. Markussen, A.-P. Jauho, and M. Brandbyge, *Nano Letters* **8**, 3771 (2008).

- ⁷K. W. Adu, Q. Xiong, H. R. Gutierrez, G. Chen, and P. C. Eklund, *Applied Physics A, Materials Science and Processing* **85**, 287 (2006).
- ⁸D. Li, Y. Wu, P. Kim, L. Shi, P. Yang, and A. Majumdar, *Applied Physics Letters* **83** (2003).
- ⁹Y. Cui, J. L. Lincoln, M. S. Gudiksen, J. Wang, and C. M. Lieber, *Appl. Phys. Lett.* **78**, 2214 (2001).
- ¹⁰N. Mingo, L. Yang, D. Li, and A. Majumdar, *Nano Letters* **3**, 1713 (2003).
- ¹¹N. Mingo and L. Yang, *Phys. Rev. B* **68**, 245406 (Dec 2003).
- ¹²O. Bourgeois, T. Fournier, and J. Chaussy, *Journal of Applied Physics* **101**, 016104 (2007).
- ¹³Y. Zhang, J. Christofferson, A. Shakouri, D. Li, A. Majumdar, Y. Wu, R. Fan, and P. Yang, *IEEE Transactions On Nanotechnology* **5** (2006).
- ¹⁴J. Chen, G. Zhang, and B. Li, *Nano Letters* **10**, 3978 (2010).
- ¹⁵J. A. Chavez, J. A. Ortega, J. Salazar, A. Turo, and M. J. Garcia, *Inst. and Meas. Tech. Conf. (IMTC)* **2**, 1019 (2000).
- ¹⁶Y. Wang, G. Chen, M. McLennan, T. S. Fisher, and T. D. Sands, “Thermoelectric Generator Module with Convective Heat Transfer,” (Jul 2010), <https://nanohub.org/resources/9153>.
- ¹⁷J. Callaway, *Phys. Rev.* **113**, 1046 (1959).
- ¹⁸M. G. Holland, *Phys. Rev.* **132**, 2461 (Dec 1963).
- ¹⁹H. Zhao, Z. Tang, G. Li, and N. R. Aluru, *Journal of Applied Physics* **99**, 064314 (2006).
- ²⁰J. Zou and A. Balandin, *Journal of Applied Physics* **89**, 2932 (2001).
- ²¹P. N. Martin, Z. Aksamija, E. Pop, and U. Ravaioli, *Nano Letters* **10**, 1120 (2010).
- ²²D. Donadio and G. Galli, *Nano Letters* **10**, 847 (2010).
- ²³Y. Zhang, J. X. Cao, Y. Xiao, and X. H. Yan, *Journal of Applied Physics* **102**, 104303 (2007).
- ²⁴I. Ponomareva, M. Menon, D. Srivastava, and A. N. Andriotis, *Physical Review Letters* **95** (2005).
- ²⁵J. C. Li, C. L. Wang, H. Peng, M. X. Wang, R. Z. Zhang, H. C. Wang, J. Liu, M. L. Zhao, and L. M. Mei, *Journal of Applied Physics* **108** (2010).
- ²⁶A. Paul and G. Klimeck, *Appl. Phys. Letts.* **98**, 083106 (2011).
- ²⁷Z. Sui and I. P. Herman, *Phys. Rev. B* **48**, 17938 (1993).
- ²⁸A. Paul, M. Luisier, and G. Klimeck, *Journal of Computational Electronics* **9**, 160 (2010).

- ²⁹J. Zi, K. Zhang, and X. Xie, Phys. Rev. B **55**, 9263 (1997).
- ³⁰S. Baroni, S. de Gironcoli, A. Dal Corso, and P. Giannozzi, Rev. Mod. Phys. **73**, 515 (Jul 2001).
- ³¹K. Parlinski, Journal of Physics: Conference Series **92**, 012009 (2007).
- ³²O. L. Lazarenkova, P. von Allmen, F. Oyafuso, S. Lee, and G. Klimeck, Applied Physics Letters **85**, 4193 (2004).
- ³³H. Fu, V. Ozolins, and Z. Alex, Phys. Rev. B **59**, 2881 (1999).
- ³⁴G. Kanellis, J. F. Morhange, and M. Balkanski, Phys. Rev. B **21**, 1543 (Feb 1980).
- ³⁵Y. F. Zhu, J. S. Lian, and Q. Jianga, “Re-examination of Casimir limit for phonon traveling in semiconductor nanostructures,” (2008).
- ³⁶P. N. Keating, Phys. Rev. **145**, 637 (1966).
- ³⁷A. Paul, M. Luisier, and G. Klimeck, 14th IEEE Workshop of Comp. Elect. DOI:10.1109/IWCE.2010.5677959(2010).
- ³⁸D. C. Wallace, Courier Dover Publications, NewYork(1998).
- ³⁹R. Landauer, IBM J. Res. Dev. **1**, 223 (1957).
- ⁴⁰J. C. Li, C. L. Wang, H. Peng, M. X. Wang, R. Z. Zhang, H. C. Wang, J. Liu, M. L. Zhao, and L. M. Mei, Journal of Applied Physics **108**, 063702 (2010).
- ⁴¹A. Palaria, G. Klimeck, and A. Strachan, Phys. Rev. B **78**, 205315 (2008).
- ⁴²Y. Xu and G. Li, Journal of Applied Physics **106** (2009).
- ⁴³O. Madelung, *Semiconductors: Data Handbook*, 3rd ed. (Springer, 2004).
- ⁴⁴W. Huang, C. S. Koong, and G. Liang, Electron Device Letters, IEEE **31**, 1026 (sept. 2010).

TABLES

TABLE I. Width Parameter for C_v in [100] SiNWs at $T = 300\text{K}$.

Shape	C_v^{bulk}	A
units \rightarrow	$(J/kg \cdot K)$	$(J \cdot nm/kg \cdot K)$
Circular	681.4	47.82
Hexagon	681.2	53.58
Square	680.9	52.66
Triangular	681.0	73.43

TABLE II. Width Parameter for C_v in SiNWs at $T = 300\text{K}$.

Orientation	C_v^{bulk}	A
units \rightarrow	$(J/kg \cdot K)$	$(J \cdot nm/kg \cdot K)$
[100]	680.9	52.66
[110]	681.5	43.03
[111]	681.2	39.4

TABLE III. Width Parameter for κ_l^{bal} in [100] SiNWs at $T = 300\text{K}$.

Shape	κ_0	(nW/K)	d
Circular	0.133		1.92
Square	0.141		1.96
Triangular	0.062		1.97
Hexagon	0.097		2.01

TABLE IV. Width Parameter for κ_l^{bal} in SiNWs at $T = 300\text{K}$.

Orientation	κ_0	(nW/K)	d
[100]	0.141		1.96
[110]	0.204		1.87
[111]	0.129		1.88

FIGURES

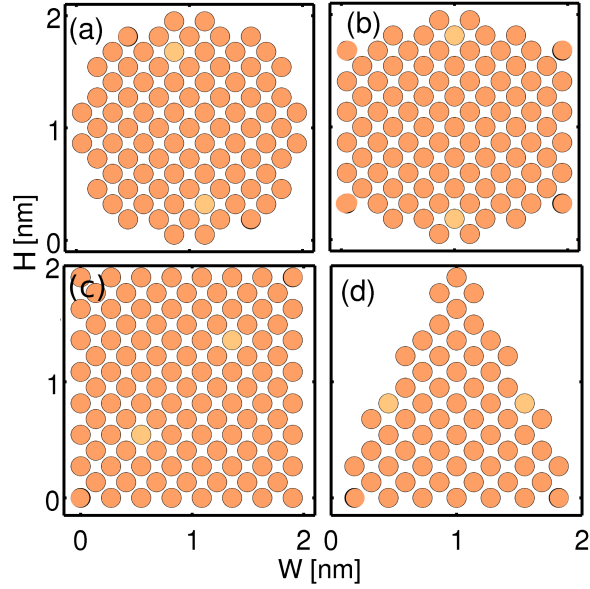


FIG. 1. Projected unit cell structures of free-standing $[100]$ oriented silicon nanowires with (a) Circular, (b) Hexagonal, (c) Square, and (d) Triangular cross-section shapes. Width and height of the cross-section are defined using a single width variable W (width = height). These structures are at $W = 2\text{nm}$.

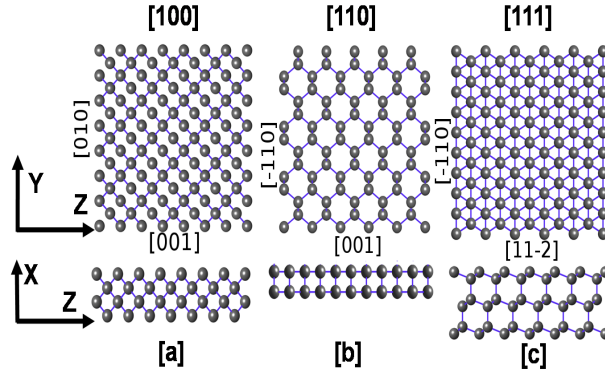


FIG. 2. Projected unit cells of square free-standing SiNWs with (a) $[100]$, (b) $[110]$, and (c) $[111]$ wire axis orientation. The width and the height of the SiNWs are defined using W . Here, $W = 2\text{nm}$.

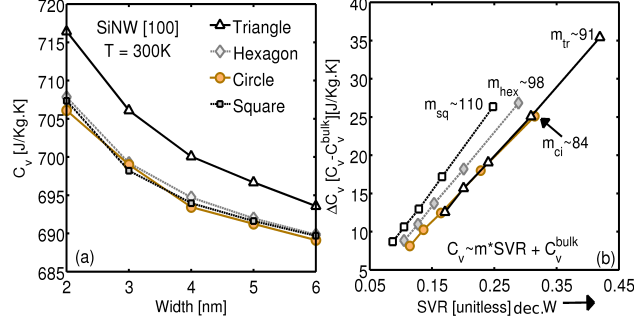


FIG. 3. (a) Dependence of the specific heat (C_v) on cross-section shape and size in [100] SiNWs. (b) Variation in ΔC_v ($= C_v - C_v^{bulk}$) with SVR for all the [100] SiNW shapes. C_v^{bulk} for each shape is given in Table. I.

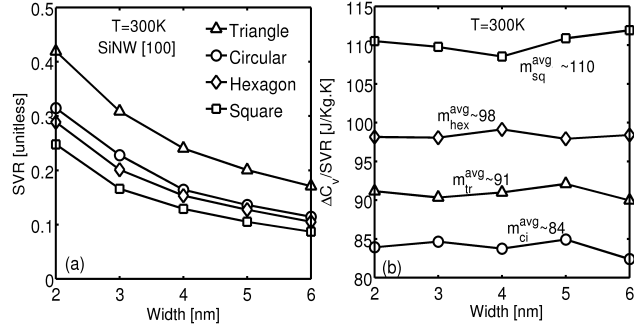


FIG. 4. (a) Surface-to-volume ratio (SVR) for different cross-section shape and size [100] SiNWs. (b) Incremental contribution to the specific heat with SVR for different cross-section shape [100] SiNWs.

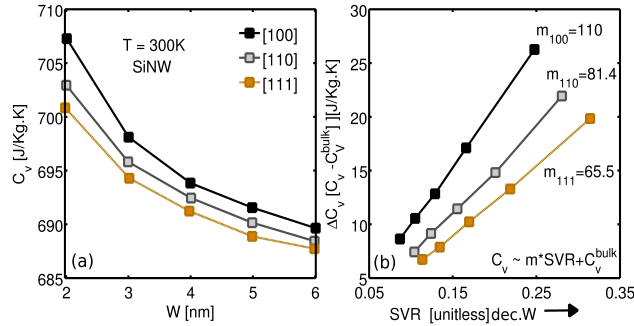


FIG. 5. (a) Dependence of the specific heat (C_v) on the orientation of square SiNWs. (b) Variation in ΔC_v ($= C_v - C_v^{bulk}$) with SVR for all the SiNW orientations. C_v^{bulk} are taken from Table. II.

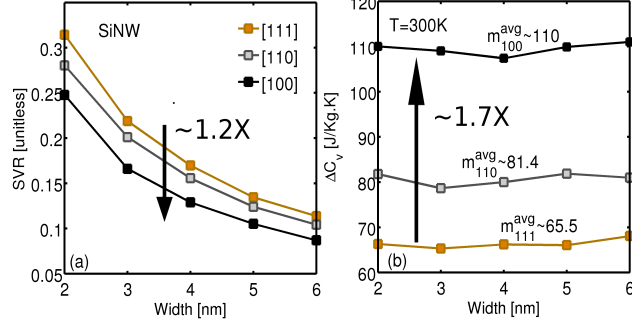


FIG. 6. (a) Surface-to-volume ratio (SVR) for different wire orientations of square SiNWs. (b) Incremental contribution to the specific heat with SVR for different orientations of SiNWs.

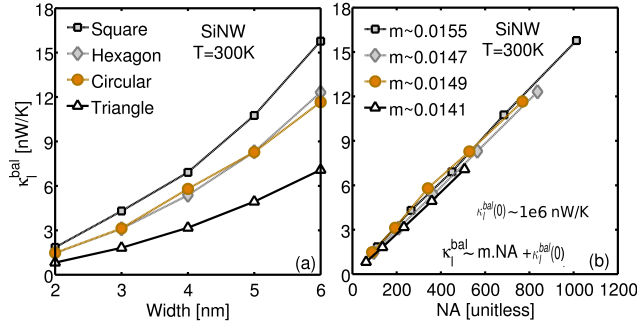


FIG. 7. (a) Effect of cross-section shape and size on the ballistic thermal conductance of [100] SiNWs. (b) Variation in κ_l^{bal} with the total number of atoms per unit cell (NA) for different cross-section shapes.

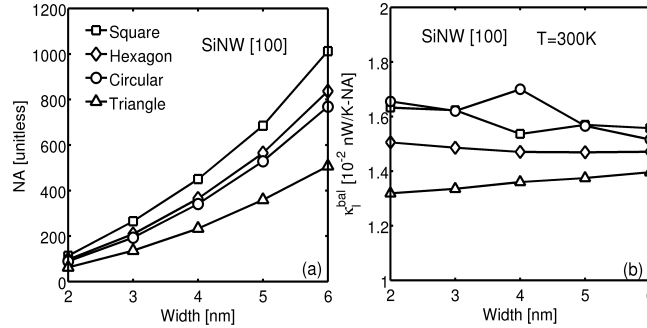


FIG. 8. (a) The number of atoms (NA) in [100] SiNW unit cell for different cross-section size and shapes. (b) Contribution to κ_l per atom for different cross-section shapes.

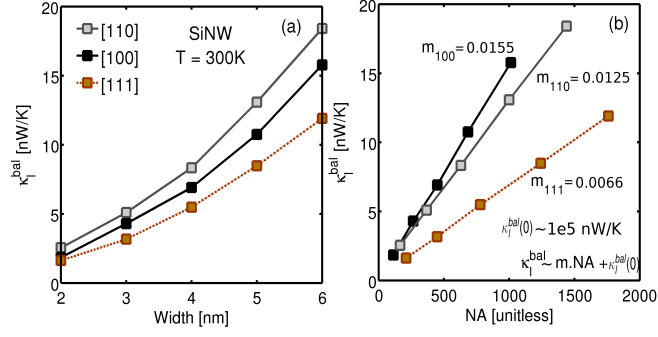


FIG. 9. (a) Effect of size on the ballistic thermal conductance in SiNWs with different orientations. (b) Variation in κ_l^{bal} with the total number of atoms in the unit cell (NA) for different wire orientations.

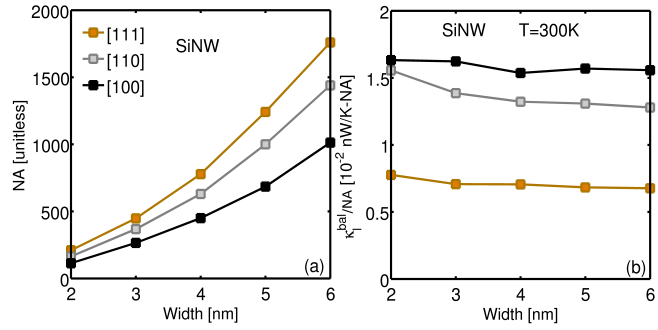


FIG. 10. (a) The number of atoms (NA) with W in one SiNW unit cell for different orientations. (b) Contribution to κ_l per atom for different SiNW orientations.

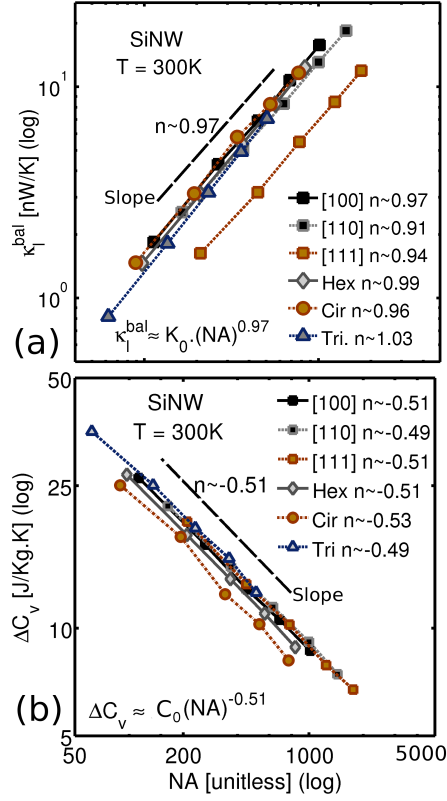


FIG. 11. (a) The number of atoms (NA) in one [100] SiNW unit cell for different cross-section size and shapes. (b) Contribution to κ_l per atom for different cross-section shapes.